JOURNAL OF NANO- AND ELECTRONIC PHYSICS
Vol. **18** No 5, 05003(5pp) (2026)

ЖУРНАЛ НАНО- ТА ЕЛЕКТРОННОЇ ФІЗИКИ
Том **18** № 5, 05003(5cc) (2026)

OPEN ACCESS

REGULAR ARTICLE

Local Laser-Enhanced Nickel Electrodeposition

V.V. Tytarenko*, V.N. Gorev, A.N. Turinov

Dnipro University of Technology, 49005 Dnipro, Ukraine

(Received 24 April 2026; revised manuscript received 25 October 2026; published online 28 October 2026)

The study presents the developed method of obtaining local nickel coatings without masks using a laser, the beam of which is focused on a cathode located in a galvanic bath. Laser acceleration of the nickel deposition process is due to the thermal effect. Probing the heat affected zone with a copper-constantan thermo-couple showed heating of the central region of the laser beam with a radius of 10 mm increases from 293 K to 371 K. The analysis of cathodic polarization curves showed that with in the laser-enhanced electrodeposition mode, an increase in the current density and a shift of the cathode potential towards positive values are observed in comparison with the deposition mode using direct current without laser irradiation. We observe an acceleration of the process of electrodeposition of nickel films by 166 times at a laser power density of 318.5 kW/m² of wavelength of 10.6 μm. The parameters of local nickel plating were calculated and the rate of electrodeposition process was estimated. The average nickel deposition rate in the area of laser irradiation is 9.6 μm/h at j = 0.77 A/dm² and E = – 0.63 V. At direct current at the given value of cathode potential (E = – 0.63 V) the nickel deposition rate is 0.06 μm/h, whereas at laser stimulation of the electrodeposition process the coating reaches this thickness (0.06 μm) in time 22 s.

Keywords: Electrodeposition, Laser radiation, Cathode overpotential, Area of thermal influence, Local electrolytic coating.

DOI: 10.21272/jnep.18(5).05003

PACS numbers: 64.70.Kd, 68.35.Bd, 68.55. Nq, 68.60.Dv, 81.15.Pq, 81.40.Ef

1. INTRODUCTION

Recently, the electrodeposition process stimulated by laser irradiation to accelerate the electrometallisation process has been the subject of increased interest of the metal coatings industry [1-4]. In the manufacturing process of microelectronic devices, existing processes for creating complex metallised structures require several particularly complex steps for mask fabrication, photolithography process, etc. This increases the complexity of process control and production cost. The development of laser-enhanced metal coating process is a very promising technology for fast maskless selective film deposition.

Application of local electrolytic nickel coatings is promising in microelectronics for the formation of conductive tracks, protective or adhesive layers, as well as for the creation of contact pads and microstructures.

The purpose of this work was to determine the optimal conditions of local laser-enhanced electrodeposition of nickel in the form of spots for the formation of contact pads or images of integrated circuit topology.

2. MATERIALS AND METHODS

Electrodeposition of nickel films was carried out from a standard sulfuric acid electrolyte of the following composition (g/l): $Ni_2SO_4 \cdot 7H_2O$ – 300, H_3BO_3 – 30, Na_2SO_4 – 50; pH = 6.

Laser electrolytic installation was used to produce nickel coatings, Fig. 1. The test installation is based on a 25 W power gas discharge continuous wave lasing CO_2-laser with wavelength λ = 10.6 microns.

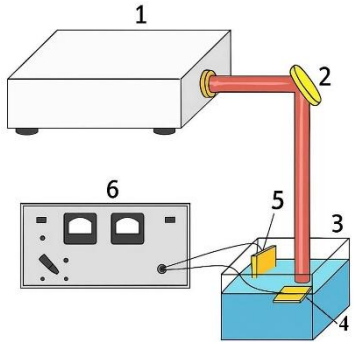


Fig. 1 – Schematic diagram of the experimental facility: radiation source (gas discharge CO_2-laser: λ = 10.6 microns, P = 25 W) (1), rotary mirror (2), electrolytic cell (3), cathode (4), anode (5), constant current source (6)

Copper substrate was used as a cathode during process of electroplating. The substrate was pre-processed in the following way. At first, it was polished mechanically by polishing paste based on chromium oxide and a diamond paste. 5 % nitric acid solution was used for chemical polishing. Chemical polishing reduced roughness and removed strain hardening resulted from mechanical polishing. After that substrates were degreased in Vienna lime to remove etching sludge and washed with distilled water. Anode was represented by

* Correspondence e-mail: tytarenko.valentina@gmail.com

© 2026 The Author(s). Journal of Nano- and Electronic Physics published by Sumy State University. This article is distributed under the terms and conditions of the Creative Commons Attribution (CC BY) license.

Cite this article as: V.V. Tytarenko et al., *J. Nano- Electron. Phys.* 18 No 5, 05003 (2026) https://doi.org/10.21272/jnep.18(5).05003

a of pure nickel plate that allowed maintaining invariable concentration of nickel ions that gave a positive effect on repeatability of tests.

The temperature of the aqueous electrolyte solution was determined using a copper-constantan thermocouple. The steady-state value of thermos-emf was established for a time of 150-200 s and measured with a digital voltmeter.

The polarization dependences were recorded in the potentiodynamic mode on a P-5827M potentiostat at a potential sweep rate of 10 mV/s. The measurements were carried out in a three-electrode electrolytic cell. A copper plate was used as the working electrode (cathode). The reference electrode was a silver chloride electrode, and the auxiliary electrode was a platinum electrode.

Transmittance spectrum of electrolyte water solutions in the IR range was recorded by spectrophotometer M80.

Metallographic studies of structure were fulfilled using microscope "Neophot-21" at magnification power x600.

3. RESULTS AND DISCUSSION

Selection of electrolyte water solution for nickel plating is based on results of investigation of transmission spectrum and distributions of temperature through thickness of solution layer in the field of radiation.

Measurement of transmission capacity of electrolyte water solutions in the middle IR-range (Fig. 2) showed that water solution has low transmission capacity in this optical band, and for CO_2-laser wavelength $\lambda = 10.6$ microns transmission factor made 10 %.

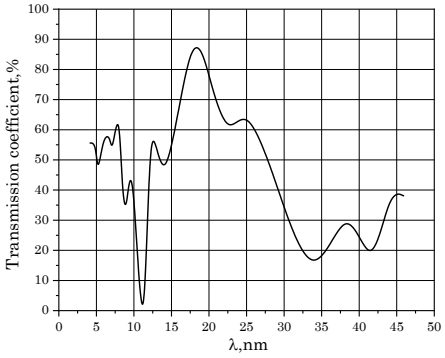


Fig. 2 – Spectral transmission graph of nickel electrolyte water solution

To prove hypothesis about local thermal effect [5-8], sounding of electrolyte water solution in conditions of laser radiation effect was fulfilled with the help of copper-constantan thermocouple (Fig. 3).

On the basis of electrolyte water solution transmission spectrum study and temperature distribution in cathode radiation area, the following conditions of electrodeposition were selected:

– nickel was electroplated subject to external enhancement by gas discharge CO_2-laser operating in medium IR-band;

– optimum thickness of electrolyte water solution layer above substrate made 5 mm.

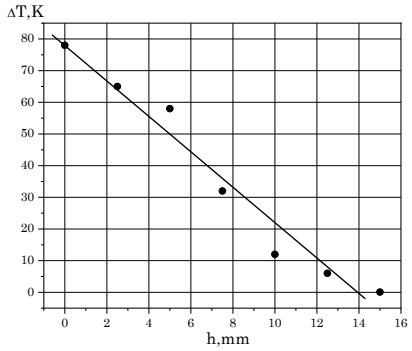


Fig. 3 – Temperature variation vs. solution layer thickness in the field of radiation

The analysis of cathodic polarisation curves (Fig. 4) showed that with increasing cathodic potential the curve of nickel reduction at switched off source of laser radiation (curve 1) is located below the curve of laser-enhanced electrodeposition process (curve 2). In the laser-enhanced electrodeposition mode, an increase in the current density and a shift of the cathode potential towards positive values are observed in comparison with the deposition mode using direct current without laser irradiation.

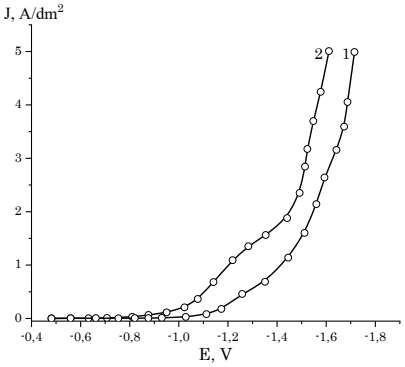


Fig. 4 – Potentiodynamic volt-ampere dependence obtained in the nickel plating electrolyte: direct current electrodeposition mode (1); laser-enhanced electrodeposition mode (2)

The efficiency of laser influence can be estimated by means of the laser acceleration coefficient, which is also a measure of the selectivity of the process and is equal to the ratio of the current density of the laser-enhanced electrodeposition mode (J) to the current density when the laser radiation source is switched off (J_0). From the cathodic polarisation curves (Fig. 4) we can see that the highest value of $K = 166$ falls on the value of the cathode potential $E = -0.63$ V for the laser power density of 318.5 kW/m^2.

Studies have shown that at potential $E > -0.75$ V nickel electrodeposition at switched off source of laser radiation is not visually observed. At $E < -0.67$ V, which corresponds to the cathode current density at laser irradiation of 0.94 A/dm^2, uniform coverage of the entire surface of the copper cathode with a layer of metallic nickel is observed.

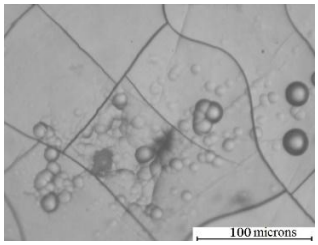
Thus, the process of local laser-enhanced electrodeposition of nickel on copper base at intensity of laser radiation of 318.5 kW/m^2 is most expedient to be carried out at cathode potential $E = -0.63$ V.

Analysis of electrodeposited nickel surface morphology showed that use of external laser exposure of cath-

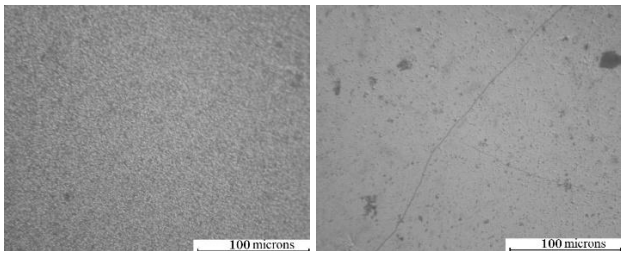
ode area in the process of electrodeposition resulted in transformation of surface morphology in comparison with coatings produced by direct current (DC) application without laser exposure (Fig. 5).

Process of cathodic nickel reduction from sulphate electrolyte is accompanied by release of hydrogen which passivates cathode surface due to adsorption across its whole surface. Analysis of DC electroplated coatings (at current density 0.5 A/dm²), showed formation of surface blisters which look like "frozen" gas bubbles and represent such superficial defects. Fig. 5 (a) shows that frozen hydrogen bubbles are internal stress concentrators and one of the factors promoting coatings cracking.

In laser-enhanced electrodeposition mode nickel coating internal stress in the radiation field decreases, coating has a developed surface (Fig. 5 b). In transition section from radiated area to non-radiated zone of the sample cracks occurred in nickel coating that testifies internal stress increase in (Fig. 5 c).



a



b c

Fig. 5 – Morphology of electroplated nickel surface: direct current electrodeposition mode (a); laser-enhanced electrodeposition mode: in radiation zone (b); out of radiation zone (c)

The increase in the deposition current density under laser irradiation is associated with local heating of the solution-electrode interface and a concomitant increase in mass transfer, which is caused by mixing of the solution near the cathode surface [5-8]. Laser acceleration of the nickel deposition process is due to the thermal effect, which was established by probing the laser irradiation zone using a copper-constantan thermocouple, which showed heating of the central region of the laser beam with radius $r_0 = 10$ mm from 296 K to 371 K.

Current density and laser acceleration coefficient of the electrodeposition process are functions of the electrolyte solution temperature (Arrhenius-type dependences):

$$J \approx \exp[W/R\,(T_0 + \Delta T)], \quad (1)$$

$$K_y \approx \exp[W\Delta T/(R(T_0 + \Delta T)T_0)], \quad (2)$$

where T_0 – temperature of the aqueous electrolyte solution, ΔT – temperature change of the aqueous electrolyte solution, W – energy of metal ions.

The energy of discharging metal ions is determined by the following expression [9, 10]:

$$W = -\alpha zF(E - E_0), \quad (3)$$

where E – the current potential value, E_0 – the equilibrium potential value ($E_0 = -0.45$ V relative to the silver chloride electrode).

Table 1 presents the energy values of the discharging nickel ions calculated by formula (3).

Table 1 – Energy of the discharging nickel ions

Deposition modes	T, K	ω, kW/m²	W, kJ/mol (eV/ion)
DC	351	–	49.6 (0,51)
Laser-enhanced electrodeposition		318.5	60.8 (0,63)

Based on the data on the stationary radial temperature distribution in the laser irradiation zone (Fig. 6), we can calculate the radial distribution of nickel electrodeposition current density:

$$J(r) = J_0 \cdot \exp\left\{\frac{E_a \cdot \Delta t(r)}{RT_0[T_0 + \Delta t(r)]}\right\}, \quad (4)$$

where $J_0 = 0{,}308$ A/m² – current density of nickel electrodeposition at $T_0 = 293$ K; $\Delta t(r)$ – temperature counted from T_0; $E_a = 42$ kJ/mol – activation energy of nickel electrodeposition, R – universal gas constant.

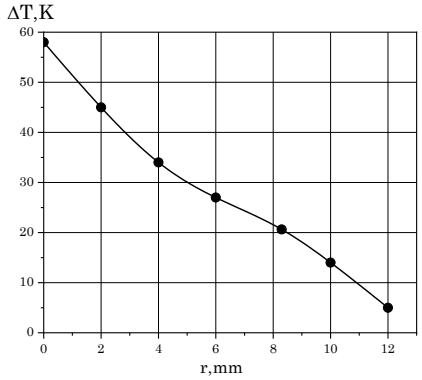


Fig. 6 – Radial temperature distribution in the laser irradiation zone

The values of current density calculated by expression (4), taking into account the data on the temperature in the laser irradiation zone (Fig. 6) and the value of the metal ion discharge energy (Table 1), are close to the values of current density for the laser-enhanced process in the central part of the laser irradiation zone. However, at $r > r_0$ (where r is a radial variable, r_0 is a laser beam radius) the temperature decreases, so the following modification of the equation is proposed to describe the radial dependence of the current density of laser-enhanced electrodeposition:

$$J(r) \cong j_0\left[1 - X(r - r_0)\frac{r - r_0}{r^* - r_0}\right] \cdot \exp\left[\frac{W \cdot \Delta T(r)}{RT_0[T_0 + \Delta T(r)]}\right], \quad (5)$$

where $JX(r - r_0) = \begin{cases} 0, r \le 0 \\ 1, r > r_0 \end{cases}$ and r^* – stationary radius of the local coating of the deposited metal.

The application of expression (5) at temperatures

corresponding to the course of the curve (Fig. 6) and the value of the metal ion discharge energy (Table 1) gives a radial profile of the current density (Fig. 7), from which we can see a decrease in the current density from the centre to the edge of the laser irradiation zone.

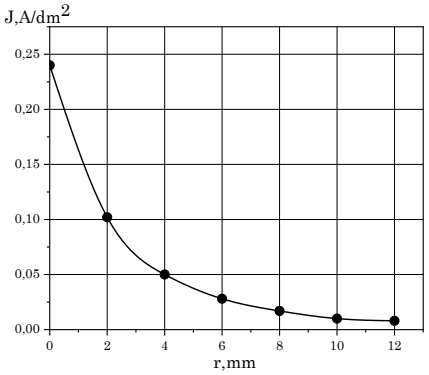


Fig. 7 – Radial current density distribution in the laser irradiation zone

In connection with the practical application of laser-enhanced electrodeposition in the technology of protective coatings [11-15], it is important to find out the radial profile of the local coating thickness of nickel films under the selected optimum conditions. The local coating thickness (d) is proportional to the current density and electrodeposition time:

$$d(r) = \frac{k}{\rho} j(r)\tau = \frac{A}{\rho F} j(r)\tau, \qquad (6)$$

where k – electrochemical equivalent ($k_{Ni} = 0.30 \cdot 10^{-6}$ kg/A·s), ρ – metal density ($\rho_{Ni} = 8800$ kg/m^3), A – atomic mass ($A_{Ni} = 58.71 \cdot 10^{-3}$ kg/mol), τ – time of the electrodeposition process, F – Faraday constant.

The results of the calculation of the local coating thickness as a function of the radial variable are shown in Fig. 8.

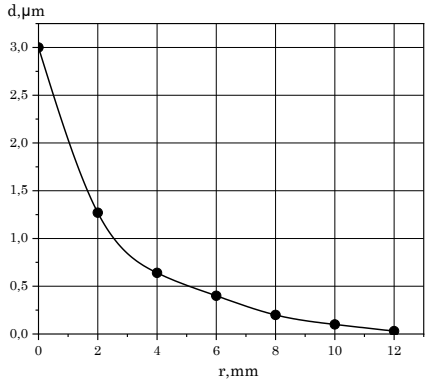
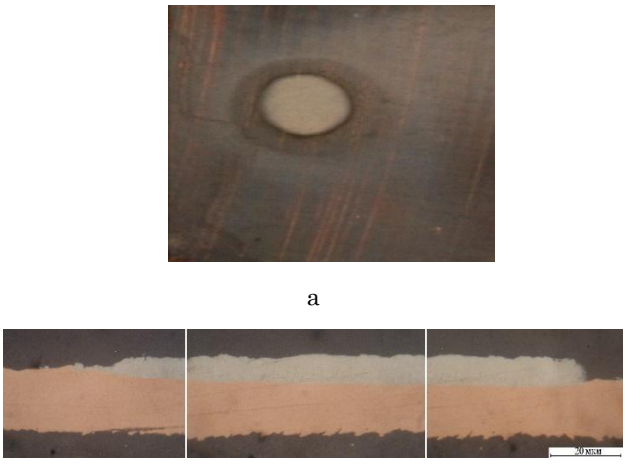


Fig. 8 – Distribution of the coating thickness depending on the radial variable

From the calculated data (Fig. 8) the thickness of the local coating decreases with increasing distance r from the centre ($r = r_0$) to the boundary of the focused laser beam and sharply decreases beyond it ($r > r_0$).

At local laser-enhanced electrodeposition of nickel, the average rate of nickel deposition in the area of the focused laser beam is 9.6 μm/h under optimal conditions of laser-enhanced electrodeposition ($J = 0.77$ A/m^2, $E = -0.63$ V), and the coating with a thickness of 0.06 μm, obtained at this potential at direct current, is deposited at laser-enhanced mode for a time $\tau \approx 22$ s.

In Fig. 9 shows the surface and cross-sectional images of the local nickel coating.



a

b

Fig. 9 – Local nickel coatings: surface (a); cross section (b)

At high values of radiation power, the temperature of the electrolyte solution in the near-cathode region significantly exceeds the temperature of the main volume of the electrolyte solution. As a result, the heated layers of the irradiation region are replaced by cooler nearby layers of the electrolyte solution and intensive mixing of the solution occurs. Convection flow leads to a decrease in the thickness of the diffusion layer at the cathode surface and to a reduction in the concentration of metal ions. Due to this, the film growth rate is significantly increased.

4. CONCLUSION

The optimal conditions for local laser electrodeposition of nickel on copper from sulfuric acid electrolyte were found, the parameters of local nickel spots were calculated, and the speed of the electrodeposition process was estimated.

After technological elaboration the obtained results can be used in maskless processes of local galvanic deposition of nickel for repair of microdefects of protective coatings of the conductive elements of printed circuit boards.

REFERENCES

1. R. Bernasconi, D. Crimella, A.G. Demir, B. Previtali, L. Magagnin, *Surf. Coat. Technol.* **484**, 130849 (2024) https://doi.org/10.1016/j.surfcoat.2024.130849.
2. J. Song, Y. Liao, C. Liu, D. Lin, L. Qiao, Y. Cheng, K. Sugioka, K. Midorikawa, S. Zhang, *J. Laser Micro Nanoeng.* **7**, 334 (2012) https://doi.org/10.2961/jlmn.2012.03.0018.
3. R. Zhou, T. Huang, L. Chen, S. Chen, S. Lin, Y. Zhuo, *J. Laser Micro Nanoeng.* **12**, 169 (2017) https://doi.org/10.2961/jlmn.2017.02.0021.
4. R.K. Gupta, A. Singh, A. Singh, P. Ram Sankar, S.K. Sharma, P.K. Mukhopadhyay, P. Ganesh, R. Kaul, K. Bindra, B. Singh, *Surf. Eng.* **34**, 446 (2018) https://doi.org/10.1080/02670844.2017.1396741.
5. Y. Yilin, Z. Jinqiu, Y. Peixia, A. Maozhong, *Mater. Rep.* **36**, 20080209-9 (2022) https://doi.org/10.11896/cldb.20080209.
6. D. Xueren, X. Kun, Z. Zhaoyang, Z. Lingyue, W. Yucheng, Z. Hao, Y. Shuai, *J. Electroanal. Chem.* **904**, 115855 (2021) https://doi.org/10.1016/j.jelechem.2021.115855.
7. X. Kun, S. Wenrong, Y. Shuai, W. Yucheng, Z. Douyan, L. Zhihao, T. Yangfan, Z. Hao, L. Sishui, Z. Zhaoyang, *Colloids Surf. A Physicochem. Eng. Asp.* **657**, 130507 (2023) https://doi.org/10.1016/j.colsurfa.2022.130507.
8. S. Wenrong, X. Kun, Z. Zhaoyang, G. Sheng, Y. Shuai, Z. Hao, L. Sishui, W. Yucheng, *J. Electrochem. Soc.* **169**, 082507 (2022) https://doi.org/10.1149/1945-7111/ac8646.
9. V.V. Tytarenko, V.O. Zabludovsky, E.Ph. Shtapenko, I.V. Tytarenko, *Phys. Chem. Solid State* **23**, 461 (2022) https://doi.org/10.15330/pcss.23.3.461-467.
10. V.V. Tytarenko, V.O. Zabludovsky, I.V. Tytarenko, *Nanosistemi Nanomater. Nanotehnologii* **22**, 41 (2024) https://doi.org/10.15407/nnn.22.01.041.
11. W. Yucheng, Y. Shuai, Z. Zhaoyang, X. Kun, L. Weining, S. Wenrong, Z. Hao, L. Yang, *Surf. Interfaces* **35**, 102458 (2022) https://doi.org/10.1016/j.surfin.2022.102458.
12. M. Xu, Z. Haiyun, Z. Yugang, H. Xingang, L. Weisheng, J. Guangfen, M. Jianbing, Z. Zengbo, Z. Jinjian, *Appl. Opt.* **62**, 1384 (2023) https://doi.org/10.1364/AO.478850.
13. Y. Wu, Z. Zhaoyang, L. Zhihao, Z. Jiabei, Y. Shuai, S. Wenrong, X. Kun, Z. Hao, L. Yang, *Appl. Surf. Sci.* **624**, 157016 (2023) https://doi.org/10.1016/j.apsusc.2023.157016.
14. W. Yucheng, Z. Zhaoyang, Z. Jiabei, Y. Shuai, X. Kun, Z. Hao, L. Yang, *Corros. Sci.* **219**, 111252 (2023) https://doi.org/10.1016/j.corsci.2023.111252.
15. W. Yucheng, Z. Zhaoyang, Z. Jiabei, Y. Shuai, X. Kun, L. Yang, S. Wenrong, *J. Manuf. Process.* **132**, 38 (2024) https://doi.org/10.1016/j.jmapro.2024.10.059.

Локальне лазерно-стимульоване електроосадження нікелю

В.В. Титаренко, В.М. Горєв, А.М. Турінов

НТУ «Дніпровська політехніка», 49005 Дніпро, Україна

В роботі представлено розроблений метод отримання локальних нікелевих покриттів без масок з використанням лазера, промінь якого фокусується на катоді, розташованому в гальванічній ванні. Лазерне прискорення процесу осадження нікелю відбувається за рахунок теплового ефекту. Зондування зони термічного впливу за допомогою мідь - константанової термопари показало нагрівання центральної області лазерного пучка радіусом 10 мм від 293 К до 371 К. Аналіз катодних поляризаційних кривих показав, що в режимі лазерного електроосадження спостерігається збільшення густини струму і зсув катодного потенціалу в бік позитивних значень у порівнянні з режимом осадження за допомогою постійного струму без лазерного випромінювання. Спостерігається прискорення процесу електроосадження плівок нікелю в 166 разів при густині лазерного випромінювання 318.5 кВт/м^2 і довжині хвилі 10.6 мкм. Розраховано параметри локального нікелювання та оцінено швидкість процесу електроосадження. Середня швидкість осадження нікелю в зоні лазерного опромінювання становить 9.6 мкм/год при J = 0.77 А/дм^2 і E = – 0.63 В. Без лазерного опромінювання при даному значенні катодного потенціалу (E = – 0.63 В) швидкість осадження нікелю за допомогою постійного струму становить 0.06 мкм/год, тоді як при лазерній стимуляції процесу електроосадження покриття досягає цієї товщини (0.06 мкм) за час 22 с.

Ключові слова: Електроосадження, Лазерне випромінювання, Катодна перенапруга, Зона термічного впливу, Локальне електролітичне покриття.